Dear Lotte Krawczyk,

Thank you very much for the comments.
As you suggested, we sorted again Chapters 2 and 3: In Chapter 2 we clarified only the method while in Chapter 3 we expanded the results together with real data example.
Now, this version is more logical and fluent for reading.

Best Regards,

Calibrating a New Attenuation Curve for the Dead Sea Region Using Surface Wave Dispersion Surveys in Sites Damaged by the 1927 Jericho Earthquake

Darvasi Yaniv[1], Agnon Amotz[1]

[1]The Fredy & Nadine Herrmann Institute of Earth Sciences, The Hebrew University of Jerusalem, 9190401, Israel

Correspondence to: Darvasi Yaniv (yaniv.darvasi@mail.huji.ac.il)

Abstract. Instrumental s~~S~~trong motion data is not common around the Dead Sea region. Therefore, calibrating a new attenuation equation is a considerable challenge. However, the Holy Land has a remarkable historical archive, attesting to numerous regional and local earthquakes. Combining the historical record with new seismic measurements will enhance the regional equation.

On 11 July 1927, a rupture, in the crust in proximity to the Northern Dead Sea, generated a moderate 6.2M_L earthquake~~On 11 July 1927, a crustal rupture generated a moderate 6.2M_L earthquake around the northern part of the Dead Sea~~. Up to five hundred people were killed, and extensive destruction was recorded, even as far as 150 kilometers from the focus. We consider local near-surface properties, in particular, the shear-wave velocity, as an amplification factor. Where the shear-wave velocity is low, the seismic intensity far from the focus would likely be greater than expected from a standard attenuation curve. In this work, we used the Multichannel Analysis of Surface Waves (MASW) method to estimate seismic wave velocity at anomalous sites in Israel in order to calibrate a new attenuation equation for the Dead Sea region.

Our new attenuation equation contains a term which quantifies only lithological effects, while factors such as building quality, foundation depth, topography, earthquake directivity, type of fault etc., remain out of our scope. Nonetheless, about 60% of the measured anomalous sites fit expectations; therefore, this new GMPE is statistically better than old ones.

From ~~a~~ our local point of view, this is the first time that integration of the 1927 historical data and modern shear-wave velocity profile measurements improves the attenuation ~~relationship~~ equation (sometimes referred to as the attenuation relation) for the Dead Sea region. In the wider context, regions of low-to-moderate seismicity should use macroseismic earthquake data, together with modern measurements, in order to better estimate the peak ground acceleration or the seismic intensities caused by future earthquakes. This integration will conceivably lead to a better mitigation of damage from future earthquakes and improve maps of seismic hazard.

1 Introduction

Generating a modern and applicable attenuation equation is one of applied seismologists main interests. Considering the Dead Sea area, for which instrumental strong motion data are not available, this task is particularly challenging. Using the Holy Land's historically rich database, researchers had defined seismic intensities and estimated earthquake locations. Investigating anomalous sites, with seismic intensities higher or lower than predicted from the basic regional attenuation relation, may lead to a better attenuation equation. The local geological conditions can strongly influence the nature and severity of shaking at a given site. Assessing the local geological conditions by geophysical techniques at these anomalous sites, and adding a logarithmic term to a basic attenuation equation, should improve the equation.

This work focuses on the 1927 event, but it is part of wider research which extends to additional earthquakes. The 1927 event was chosen as it is the only devastating one recorded, albeit teleseismically, during the instrumented period.

Our main goal in this research is a tighter constraint on the attenuation equation derived from this event. This should allow us to examine whether this preliminary work coincides with our expectations of site amplification and de-amplification due to the local lithology.

1.1 Site Response

Ground motion is controlled by a number of variables, including source characteristics, source distance, propagation directivity, near-surface geology, etc. The elastic properties of near-surface materials, and their effect on seismic wave propagation, are crucial to earthquake and civil engineering, and environmental and earth science studies.

Seismic surface waves are initiated at the moment that the earthquake wave front impinges on the surface. These waves spread out, and the surface shakes as they pass. Surface wave amplitude at the surface is controlled by the mechanical properties of the rocks below. These often consist of low velocity weathered rock over bedrock with much higher velocities. When seismic waves pass from a high-velocity layer to a low-velocity layer, their amplitudes and duration typically increase. The phenomena of site amplification, as a result of soft sediments overlying hard bedrock, is well known since the early days of seismology (Milne, 1898). Site-effects are also well known and were investigated after several major earthquakes: Mexico City 1985 (Singh et al., 1988), Yerevan 1989 (Borcherdt et al., 1989), San Francisco 1989 (Hough et al., 1990), Los Angeles 1994 (Hall et al., 1994) and Kobe, 1995 (Aguirre and Irikura, 1997). Therefore, local lithology is a crucial factor for estimating site amplification, defined as the amplitude ratio between the surface layer and the underlying bedrock. Site amplification at a specific site can be attributed to many factors, such as basin effects, focusing effects, topography, and reverberation of the seismic waves in the upper layers due to acoustic impedance differences (Figure 1).

The amplification, *A*, is proportional to the reciprocal square root of the product of the shear-wave velocity, *Vs*. (Eq. (1)) (Aki and Richards, 2002):

$$A \propto \frac{1}{\sqrt{V_s \rho}}, \quad (1)$$

where ρ is the density of the investigated soil. As shear-wave velocity decreases by a given fraction the amplification increases by half that fraction (for a constant density). Since density plays a minor role (Dal Moro, ~~2015~~2014; Xia et al., 1999) the V_s value can be used to represent site conditions.

The most widely used index in the classification of the soil response is the average shear-wave velocity in the uppermost 30 meters, the Vs_{30}. This index was accepted for site classification in the USA – National Earthquake Hazards Reduction Program – NEHRP (Building Seismic Safety Council, 2001). In Europe by the new provisions of Eurocode 8 (BSI, 2011), and in Israel it is accepted by the design provisions for earthquake resistance of structures - SI 413 (The Standards Institution of Israel, 2013). The value of 30 meters comes from the USA and European building codes, where it was found empirically that this depth is directly proportional to deeper and shallower values (Boore et al., 2011). Zaslavsky et al. (2012) argued that the use of Vs_{30} is a simplification that cannot be justified in the complex geological conditions in Israel, yet no alternatives have thus far been proposed. Therefore, in this scenario, the Israel Standards Institute still adopts the Vs_{30} index.

In modern attenuation equations, also known as ground motion prediction equations (GMPE), coefficients are derived from strong motion data, namely from ground acceleration measurements. In the past, and in areas lacking the technology to record earthquakes, it was impossible to measure the peak ground acceleration (PGA) directly. Therefore, it is common to categorize historical earthquakes with seismic intensity scales that describe the damage at each site or area (Ambraseys, 2009; Guidoboni and Comastri, 2005)

1.2 The M6.2 1927 Jericho earthquake

The left-lateral Dead Sea transform separates the Sinai-Levant Block from the Arabian Plate (Figure 2). The 6.2M_L July 11, 1927, Jericho earthquake (Ben-Menahem et al., 1976; Shapira, 1979) was the strongest and most destructive earthquake to hit the Holy Land during that century. Furthermore, it was the first to be instrumentally recorded by seismographs. The epicentral location was originally estimated at a few kilometers south of the Damia Bridge, which is 30 kilometers north of Jericho (International Seismological Summary – ISS Bulletin of 1927). In the following decades new estimates have been published: Shapira et al. (1993) calculated the epicenter to be near Mitzpe Shalem. Zohar and Marco (2012) estimated the epicenter to be near the Almog settlement, about 30 kilometers north of Shapira's epicenter, and Kagan et al. (2011), surmised that the source was somewhere on the Kalia fault, located in the northern part of the Dead Sea graben, perpendicular to the main Dead Sea fault (Figure 2).

The damage from the earthquake was heavy, especially in places near the source, but not only there: In Nablus, located 70 km from the epicenter (Figure 2), 60 people were killed, 474 were injured, and more than 700 structures were destroyed, most of which were built on soft sediments (Blankenhorn, 1927; Willis, 1928). By comparison, Jerusalem is only about 30 kilometers from the source and the damage there was much smaller, especially in property. However, in Mount Scopus and the Mount of Olives (eastern neighborhoods in Jerusalem), the damage exceeded that in other parts of Jerusalem (Abel, 1927; Brawer, 1928). Other cities also suffered from this earthquake: Tens of people were injured and even died, and hundreds of houses were ruined in Ramleh and Lod (Brawer, 1928). Jericho in the Jordan Valley also suffered significant damage, especially in terms of buildings collapsing (Figure 3). The total number of victims was about 350-500 (Ambraseys and Melville, 1988; Amiran, 1951; Arieh, 1967; Ben-Menahem, 1991). Beyond the casualties, several environmental effects were reported: The Jordan river flow ceased near the Damia bridge for about 21.5 hours (Willis, 1928) and a one-meter seiche wave was observed in the Dead Sea (Abel, 1927; Blankenhorn, 1927). Some evidence suggests that the earthquake was felt up to 700 kilometers from the epicenter (Ben-Menahem, 1991), although a different interpretation suggests this distance was only 300 kilometers (Ambraseys and Melville, 1988).

Compiling historical evidence, Avni (1999), in his PhD thesis, estimated the seismic intensities (MSK or Medvedev-Karkik-Sponheuer scale (Medvedev et al., 1965))~~scale~~) at 133 different locations around Israel, Palestine, Jordan, Lebanon, Syria, and Egypt (Figure 4 and for locations and S~~s~~upplementary). The curve that Avni (1999) fit to his scattered *MSK* vs *d* points, represents his basic attenuation equation, and had an R^2 of about 0.26. Based on the methodology proposed by Bakun and Wentworth (1997), Hough and Avni (2011) published a new attenuation equation for the Dead Sea region:~~Avni's (1999) basic attenuation equation yields an R^2 of about 0.26. Based on the methodology proposed by Bakun and Wentworth (1997), Hough and Avni (2011) revised the attenuation equation for the Dead Sea region:~~

$$MMI(M,d) = -0.64 + 1.7M - 0.00448d - 1.67\log(d) \quad (2)$$

where *MMI* is the Modified Mercalli Intensity (assumed to be equivalent to MSK), *M* is the magnitude and *d* is the distance from the epicenter.

~~Raphael and Agnon (2018) note that damage from the 1927 Jericho earthquake was higher east of the transform (on the Arabian Plate) than on the west (Sinai-Levant Block). This observation, consistent with their archaeoseismic findings for earthquakes in antiquity, requires further study.~~

2 Methods - Multichannel Analysis of Surface Waves (MASW)

2.1 MASW Theory

The MASW method is environmentally friendly, non-invasive, low-cost, rapid, robust, and provides reliable Vs_{30} data (Miller et al., 2002). Multichannel records make it possible to separate different wavefields in the frequency and velocity domains. Fundamental and higher modes can be analyzed simultaneously, but generally, only the fundamental mode is used because it has the highest energy (Park et al., 1998).

The MASW method consists of three main steps: (A) Acquisition of experimental data, (B) signal processing to obtain the experimental dispersion curve, and (C) inversion to estimate Vs_{30} (Figure 5). The inverse problem consists of estimating a set of parameters that describe the soil deposit, based on an experimental dispersion curve. Inversion problems based on wave propagation theory cannot be solved in a direct way due to their non-linearity. Thus, iterative methods must be used where a theoretical dispersion curve is determined for a given layer model and compared to the previously obtained experimental dispersion curve (Ryden et al., 2004). Vs_{30} typically does not converge to one stable value. In other words, for the same dispersion curve, one will get slightly different Vs_{30} depending on the initial model. ~~Yet, the ensuing uncertainty is of little consequence since Vs_{30} enters logarithmically into the attenuation equation (see below).~~

~~We carried out the surveys with a linear array of 24 vertical geophones (R.T. Clark's geophones with natural frequency of 4.5 Hz) at equal intervals of 2-3 meters over a total length of 46-69 meters. For the survey sound source we used a five-kilogram sledgehammer striking a twenty-centimeter square aluminum plate at variable offsets of 5, 10, 15, 20, 25 and 30 meters (both forward and reversed). The seismic data were recorded on a Geometrics Geode seismograph at a sampling rate mostly of 8 kHz for 0.5-2 seconds (Table 1). For an acceptable Signal to Noise Ratio, we used the so-called "vertical stacking" approach, which is a summation of multiple synchronized repetitions of the test (usually five times).~~

~~Rayleigh wave dispersion curves are obtained by the MASW module of the RadExPro® software, whose calculation procedure is based on a paper by Park et al. (1998), and also by the WinMASW® software. From all the dispersion images that we calculated from each offset shot (Figure 6), we choose the smoothest and clearest one (Figure 6) to compute the site's Vs_{30} profile. An inversion process then finds the shear-wave velocity profile whose theoretical dispersion curve is as close as possible to the experimental curve (Figure 6). The data and coefficients are automatically inverted via genetic algorithms which represent an optimization procedure belonging to the classification of global search methods. Genetic algorithms are commonly used to generate high-quality solutions to optimization and search problems by relying on bio-inspired operators such as mutation, crossover and selection. Compared to traditional linear inversion methods based on gradient methods (Jacobian matrix) these inversion techniques produce a very reliable result in terms of precision and completeness (Moro et al., 2007).~~

2.2 Velocity model

All models were considered to be a stack of homogeneous linear elastic layers, neglecting lateral variations in soil properties. The number of unknowns for a layered model, when considering only shear-wave velocity, is three for each layer: density, thickness, and one elastic constant. Therefore, the number of unknowns is $3n$-1 (where n represents the number of layers). The change in density with depth is usually small in comparison to the change in shear modulus and is normally neglected (Park et al., 1997).

2.3 Number of layers & layer thicknesses

The resolution of surface wave surveys decreases with depth. Thin layers are well resolved when they are close to the surface, whereas at great depth, the resolution is limited and only large changes can be detected (Foti et al., 2014). Regardless of the number of the layers of the site, Vs_{30} is almost the same in each case (Figure 7). For those reasons, as well as the lack of density information, we did not restrict each model to a specific number of layers. Without boreholes and lithostratigraphic data, which is the case in our work, a useful rule of thumb is to assume layer thicknesses increasing with depth, to compensate for the decreased resolution with depth, an intrinsic shortcoming of surface wave testing (Foti et al., 2014).

2.4 Depth of investigation

We used a five-kilogram sledgehammer and summed up five strikes. For some sites, this type of source is insufficient to determinate a shear-wave profile down to 30 meters. In addition, at some sites, we were not able to spread the geophones at intervals of more than two meters, which limited the length of the seismic line. This length probably excludes longer wavelengths which limits the depth of investigation. Lastly, as the shear-wave velocity of the lowest frequency is higher – more data is available for deeper layers. Therefore, the penetration depth will decrease in areas with low shear-wave velocity. For instance, if we can clearly detect a phase velocity of about 300 m/sec at 5 Hz, we can roughly estimate a depth of investigation of approximately 20-30 meters according to the following equation:

$$Z = \frac{\left(\frac{Velocity_{f_{\min}}}{f_{\min}}\right)}{n}, \quad (3)$$

where n equals 2-3 (Foti et al., 2014; Moro, 2015). In other words, this equation emphasizes that the depth of investigation is about a half to a third of the largest wavelength observed.

3 Results

We carried out the surveys with a linear array of 24 vertical geophones (R.T. Clark's geophones with a natural frequency of 4.5 Hz) at equal intervals of 2-3 meters over a total length of 46-69 meters. For the survey sound source we used a five-kilogram sledgehammer striking a twenty-centimeter square aluminum plate at variable offsets of 5, 10, 15, 20, 25 and 30 meters (both forward and reversed) (Figure 6A). The seismic data were recorded on a Geometrics Geode seismograph at a sampling rate mostly of 8 kHz for 0.5-2 seconds (Table 1). For an acceptable Signal to Noise Ratio, we used the so-called "vertical stacking" approach, which is a summation of multiple synchronized repetitions of the test (usually five times).

Rayleigh wave dispersion curves are obtained by the MASW module of the RadExPro® software, whose calculation procedure is based on a paper by Park et al. (1998), and also by the WinMASW® software. From all the dispersion images that we calculated from each offset shot (Figure 6B), we choose the smoothest and clearest one (Figure 6C) to compute the site's Vs_{30} profile. An inversion process then finds the shear-wave velocity profile whose theoretical dispersion curve is as close as possible to the experimental curve (Figure 6D). The data and coefficients are automatically inverted via genetic algorithms which represent an optimization procedure belonging to the classification of global-search methods. Genetic algorithms are commonly used to generate high-quality solutions to optimization and search problems by relying on bio-inspired operators such as mutation, crossover and selection compared to traditional linear inversion methods based on gradient methods (Jacobian matrix) these inversion techniques produce a very reliable result in terms of precision and completeness (Dal Moro et al., 2007).

From 24 surveys, we succeeded in extracting Vs_{30} for 19 of the 20 sites studied (the Hartuv data were too noisy for interpretation) (Table 2 and Supplementary). These would be used to recalibrate the attenuation equation arrived at by previous investigators at 133 sites19 of the 133 sites

3.1 Velocity model

All ground models were considered to be a stack of horizontal homogeneous elastic layers, neglecting lateral variations in soil properties. The number of unknowns for a layered model, when considering only shear-wave velocity, is three for each layer: density, thickness, and one elastic constant. Therefore, the number of unknowns is $3n$-1 (where n represents the number of layers). The change in density with depth is usually small in comparison to the change in shear modulus and is normally neglected (Park et al., 1997).

3.2 Number of layers & layer thicknesses

The resolution of surface wave surveys decreases with depth. Thin layers are well resolved when they are close to the surface, whereas at great depth, the resolution is limited and only large changes can be detected (Foti et al., 2014). Regardless of the number of the layers at the site, Vs_{30} is almost the same in each case (Figure 7). For these reasons, as well

as the lack of density information, we did not restrict each model to a specific number of layers. Without boreholes or other direct lithostratigraphic constraint, which is the case in our work, a useful rule of thumb is to assume layer thicknesses increasing with depth, to compensate for the decreased resolution with depth, an intrinsic shortcoming of surface wave testing (Foti et al., 2014).

3.3 Depth of investigation

We used a five-kilogram sledgehammer and summed up five strikes. For some sites, this type of source is insufficient to determinate a shear-wave profile down to 30 meters. In addition, at some sites, we were not able to spread the geophones at intervals of more than two meters, which limited the length of the seismic line. This length probably excludes longer wavelengths which limits the depth of investigation. Lastly, as the shear-wave velocity of the lowest frequency is higher - more data is available for deeper layers. Therefore, the penetration depth will decrease in areas with low shear-wave velocity. For instance, if we can clearly detect a phase velocity of about 300 m/sec at 5 Hz, we can roughly estimate a depth of investigation of approximately 20-30 meters according to the following equation:

$$Z = \frac{\frac{Velocity_{f_{min}}}{f_{min}}}{n}, \quad (3)$$

where n ranges between 2 and 3 (Foti et al., 2014; Dal Moro, 2014). In other words, this equation emphasizes that the depth of investigation is about a half to a third of the largest wavelength observed.

3.4 Recent improvement of the 1927 epicenter

Zohar and Marco (2012) relocated the 1927 epicenter to a point near the Almog settlement. We used this most recently published epicenter to calculate new epicentral distances for the 133 sites. Since Equation 2 above is dependent upon *d*, we checked the variable scatter in the points, but found that the changes in the best-fit coefficients were very minor, so that we assumed for all purposes to use the original.

Figure 8 shows a scatter plot of the original *MMI* (assumed equivalent to MSK) vs. new *d* for their 133 sites. Hough and Avni (2011) fit this data with a curve whose equation best describes the attenuation equation for this event. Using the mathemathical form of their curve, we calculated upper and lower limits such that 60% of the points are enclosed. This we call the 60% prediction boundary. We consider that the lithological effects probably account for much of the scatter beyond this boundry, due to amplification and de-amplification.

~~Zohar and Marco (2012) relocated the epicenter to a point near the Almog settlement. We used this most recently published epicenter for calculating the new epicentral distances, *d*. Figure 8 shows a scatter plot of *MMI* vs. *d* for their 133 sites. Hough and Avni (2011) fit this data with a curve which best describes the attenuation relation for this event. Using the mathemathical form of their curve, we calculated upper and lower limits such that 60% of the points are enclosed. This we call the 60% prediction boundary. We consider that the lithological effects probably account for much of the scatter beyond this boundry, due to amplification and de-amplification.~~

~~**3.1 MASW surveys**~~

~~From 24 surveys, we succeeded in extracting Vs_{30} for 19 of 20 sites (the Hartuv data were too noisy for interpretation) (Table 2 and Supplementary).~~

4 Discussion

A number of researchers have studied the 1927 event. Avni (1999) tried to reduce the impact of local geology and attempted to generate basic attenuation curves for specific azimuths. Zohar and Marco (2012) relocated the source position while Shani-Kadmie et al. (2016) studied directivity of the source pattern. None of these publications address the Vs_{30} measurements. An attenuation equation with a term that depends on the Vs_{30} index should lead to a better understanding of past events, and to more useful predictions of future earthquakes.

4.1 Survey locations and validation

The decision as to where exactly each survey should take place was based on Avni's thesis (Avni, 1999). Where the location was not sufficiently known, we rechecked the reference given by Avni. In most cases, there was evidence of specific damaged buildings. We tried to locate these buildings on historical maps (1927-1945). Unfortunately, most sites were located inside urban areas, where we could not carry out the seismic surveys. Therefore, we surveyed in nearby open areas as close as possible to the referenced damage zones.

To validate our results, we compared them with a summary of thousands of seismic evaluations around Israel carried out over the years by the Geophysical Institute of Israel (GII), and compiled in a report by (Aksinenko and Hofstetter, 2012). These evaluations were based upon refraction and borehole velocity measurements yielding *Vs* and/or *Vp* values, as well as the effects of topography and geology. The spacing of their data was such that often a number of GII sites had to be averaged to provide a value within several kilometers for comparison with our MASW values. However, Figure 9 shows that the GII-based values are in consistent agreement with those of the MASW. However, this comparison is a bit tricky because Vs_{30} results for two sites 5 km or much less distant could be significantly different, as shown in Figure 10. Remembering that Vs_{30} enters a logarithmic term, we find our approach potentially useful.

Table 2 lists our 24 sites alphabetically, with their respective Vs_{30} values, the computed errors, and epicentral distances, *d*. The Vs_{30} values vary from a low of 232 m/sec in Beit Alfa, -85 m.s.l. (Figure 11), in the thick and active alluvial plain of the famous Valley of Gilboa some 10 km from the Dead Sea rift, and a site of many millennia of agriculture. The highest value is 1,444 m/sec in Peqi'in, 680 m.s.l (Figure 11). in an area of ancient hillside orchards, and massive carbonate bedrock. On the other hand, the two Motza sites (Figure 11) lie in Emeq HaArazim (Valley of the Cedars) on the western flank of Jerusalem within the massive anticlinorium of the Judean Hills, at about 570 m.s.l.. Motza 1 (1065 m/sec) is on a compacted

dirt parking lot above alluvium and the Soreq Fm., while Motza 2 (874 m/sec) is farther up the valley on a gentle hillside above the Bet Meir Fm.. Both are of similar limestone and marl composition and Cretaceous age.

4.2 A new attenuation equation

In the present case of the 1927 earthquake, the sources of the data are mostly historical documents and not strong data measurements. This makes it difficult to quantify site response into a single equation. In the practical modern attenuation relationship, Vs_{30} is a crucial index. A term that depends on Vs_{30} has previously been constrained for several large data sets (Abrahamson et al., 2014; Boore et al., 1997; Campbell and Bozorgnia, 2008). We chose the Boore et al. (1997) attenuation equation (Eq. (4)) in order to emphasize site response:

$$\ln Y = b_1 + b_2(M-6) + b_3(M-6)^2 + b_5 \ln(\mathrm{r}) + b_v \ln\left(\frac{Vs}{V_A}\right), \quad (4)$$

where Y is the ground-motion variable (peak horizontal acceleration or pseudo-acceleration response in g), M is the moment magnitude, r is the epicentral distance in kilometers, V_A, and all b terms are frequency dependent coefficients to be determined. By adding Boore et al.'s (1997) Vs term to Hough and Avni (2011) attenuation equation (Eq. (2)), we suggest a new equation for the region:

$$MMI = -0.64 + 1.7M - 0.00448d - 1.67\log(d) + C_4 \ln\left(\frac{Vs_{30}}{V_A}\right), \quad (5)$$

where V_A and C_4 are adjustable coefficients. The first four coefficients remain the same as we assert that the magnitude, attenuation, geometrical spreading and site response are all independent. We adopt the value of V_A from Boore's (1987) equation (Eq. (4)), as it represents a single value independent of the frequency. We took formerly derived GMPE, with its coefficients, and added another term, by regressing only for the new coefficient, then optimizing C_4 and V_A by Least Squares Fitting (LSF), as shown in ~~Figure 11~~ Figure 12 we get the final equation:

$$MMI = -0.64 + 1.7M - 0.00448d - 1.67\log(d) - 2.1\ln\left(\frac{Vs_{30}}{655}\right), \quad (6)$$

4.3 The performance of the new attenuation equation

With these coefficients, 58% or 11 of 19 sites, were amplified or de-amplified as we expected. For the entire distance range (up to 250 km) the Vs_{30} corrections leave 42% sites out of the prediction boundary (eight of nineteen sites). Seismic intensities at all these eight sites are overpredicted by the attenuation equation (Eq. (2)) (~~Figure 12~~Figure 13). We expect that Vs_{30} at these sites will be higher than 655 m/sec in order to obtain de-amplification. However, our results show the opposite effect - these eight sites are characterized by lower Vs_{30} which drives amplification. This can be caused by the fact that measurements were taken over agricultural fields, of which the upper layers (the first few meters) are characterized by low

shear-wave velocity, decreasing the average *Vs*. Another reasonable explanation is that we did not succeed in extracting the average shear-wave velocity down to 30 meters and perhaps we missed some high-velocity shear-wave layers at deeper layers. In such cases, we constrain the last layer to be thicker in order to estimate Vs_{30} for all our surveys.

5 Conclusions

In this research, we investigate site amplification and de-amplification around Israel. According to previous studies (Aki, 1988; Boore, 2003; Borcherdt, 1994; Field and Jacob, 1995; Joyner and Boore, 1988), the local lithology can amplify or de-amplify wave amplitude. The commonly used modern seismic method – MASW – allowed the extraction of *Vs* profiles at 19 sites reportedly damaged by the 1927 M_L6.2 earthquake. We use these profiles to update the attenuation equation for the Dead Sea region by including the Vs_{30} term.

According to this new equation, 11 sites, which constitute 58% of our measured samples, move into the 60% prediction boundary. This suggests that the prediction boundary actually encompasses over 80% of the macroseismic observations. This fit is better than any available attenuation equation for the Dead Sea region. However, as we have used only 19 sites, we should consider further research and provide wider results. Although our final equation (Eq. (6)) shows amplification and de-amplification depending on Vs_{30}, it does not take into consideration any other factor, such as building quality, foundation depth, topography, earthquake directivity, type of fault, etc. Obviously, for better results, we must use additional methods and jointly invert some other seismic data such as: refraction (S and P waves), Horizontal to Vertical Spectral Ratio (HVSR), MASW of the transverse component of Love waves, MASW of the radial component of Rayleigh wave, Extended Spatial Auto-Correlation (ESAC), etc. Also, with these data in hand, a full inversion for the epicenter will be in order.

Despite the scarcity of data, this is the first time that an integration of historical data with shear-wave velocity profile measurements improves the attenuation relation. In order to better estimate the peak ground acceleration or the seismic intensities that will be caused by future earthquakes, attenuation relations are necessary for areas characterized by high seismicity. Some of the regions of low to moderate seismicity have rich sources of historical earthquake data. The integration of historical data with modern shear-wave velocity profile measurements will lead to a better understanding of future earthquakes.

Acknowledgments. We thank the Neev Center for Geoinfomatics's facilities and its students. We are especially grateful to Dr. John K. Hall, founder of the Center, for his ongoing support. We are grateful to the Helmholtz Association of German Research Centers for funding this research. We thank Prof. Moshe Reshef for comments and suggestions on an earlier draft and Prof. Ran Bachrach for valuable advice. We acknowledge the contribution of Prof. Michael Weber and the geophysical deep sounding section at GFZ. Finally, we thank Amit Ronen for his assistance.

References

Abel, F. M.: No Le Recent Tremblement de Terre en Palestine, Rev. Biblique, 36, 571–578, 1927.

Abrahamson, N. A., Silva, W. J. and Kamai, R.: Summary of the ASK14 ground motion relation for active crustal regions, Earthq. Spectra, 30(3), 1025–1055, 2014.

Aguirre, J. and Irikura, K.: Nonlinearity, liquefaction, and velocity variation of soft soil layers in Port Island, Kobe, during the Hyogo-ken Nanbu earthquake, Bull. Seismol. Soc. Am., 87(5), 1244–1258, doi:10.1144/pygs.51.3.177, 1997.

Aki, K.: Local site effects on ground motion, Earthq. Eng. Soil Dyn. II-Recent Adv. Gr. Motion Eval. Geotech. Spec. Pudlication, 20, 103–155, 1988.

Aki, K. and Richards, P. G.: Quantitative seismology, University Science Books., 2002.

Aksinenko, T. and Hofstetter, A.: 1-D semi-empricical modeling of the subsurface across Israel for site effect evaluations., 2012.

Ambraseys, N.: Earthquakes in the Mediterranean and Middle East: a multidisciplinary study of seismicity up to 1900, Cambridge University Press., 2009.

Ambraseys, N. N. and Melville, C. P.: An analysis of the eastern Mediterranean earthquake of 20 May 1202, Hist. Seism. earthquakes world, 181–200, 1988.

Amiran, D. H. .: A Revised Earthquake-Catalouge of Palastine, Isr. Explor. J., 2, 48–65, 1951.

Arieh, A.: Seismicity of Israel and Adjacent Area, Minist. Dev., 43, 1–14, 1967.

Avni, R.: The 1927 Jericho Earthquake. Comprehensive Macroseismic Analysis Based on Contemporary Sources., Ben Gurion University of the Negev, Beer Sheva (in Hebrew)., 1999.

Bakun, W. H. and Wentworth, C. M.: Estimating earthquake location and magnitude from seismic intensity data, Bull. Seismol. Soc. Am., 87(6), 1502–1521, 1997.

Ben-Menahem, A.: Four thousand years of seismicity along the Dead Sea Rift, J. Geophys. Res., 96(B12), 20195, doi:10.1029/91JB01936, 1991.

Ben-Menahem, A., Nur, A. and Moshe, V.: Tectonics, seismicity and structure of the Afro - Eurasian junction - the breaking of an incoherent plate, , 12(1), 1–50, 1976.

Blankenhorn, M.: Das Erdbeben in Juli 1927 in Palestina, Zeitschr.D.Pal, (51), 123–125, 1927.

Boore, D. M.: Simulation of ground motion using the stochastic method, Pure Appl. Geophys., 160(3), 635–676, doi:10.1007/PL00012553, 2003.

Boore, D. M., Joyner, W. B. and Fumal, T. E.: Equations for Estimating Horizontal Response Spectra and Peak Acceleration from Western North American Earthquakes: A Summary of Recent Work, Seismol. Res. Lett., 68(1), 128–153, doi:10.1785/gssrl.76.3.368, 1997.

Boore, D. M., Thompson, E. M. and Cadet, H.: Regional correlations of Vs30 and velocities averaged over depths less than and greater than 30 meters, Bull. Seismol. Soc. Am., 101(6), 3046–3059, doi:10.1785/0120110071, 2011.

Borcherdt, R., Glassmoyer, G., Andrews, M. and Cranswick, E.: Effect of site conditions on ground motion and damage, Earthq. spectra, 5(S1), 23–42, 1989.

Borcherdt, R. D.: Estimates of site-dependent response spectra for design (methodology and justification), Earthq. spectra, 10(4), 617–653, 1994.

Brawer, A. Y.: Earthquakes events in Israel from July 1927 to August 1928, 1928.

BSI: Eurocode 8 : Design of structures for earthquake resistance, 3, 2011.

Building Seismic Safety Council: NEHRP Recomendations for Seismic Regulations for New Buildings and Other Structures, Part 1 : Provisions (FEMA - 368), (Fema 368), 392, 2001.

Campbell, K. W. and Bozorgnia, Y.: NGA ground motion model for the geometric mean horizontal component of PGA, PGV, PGD and 5% damped linear elastic response spectra for periods ranging from 0.01 to 10 s, Earthq. Spectra, 24(1), 139–171, doi:10.1193/1.2857546, 2008.

Ciaccio, M. G. and Cultrera, G.: Terremoto e rischio sismico, Ediesse., 2014.

Field, E. H. and Jacob, K. H.: A comparison and test of various site-response estimation techniques, including three that are not reference-site dependent, Bull. Seismol. Soc. Am., 85(4), 1127–1143, 1995.

Foti, S., Lai, C., Rix, G. and Strobbia, C.: Surface Wave Methods for Near-Surface Site Characterization., 2014.

Guidoboni, E. and Comastri, A.: Catalogue of Earthquakes and Tsunamis in the Mediterranean Area from the 11th to the 15th Century, Istituto nazionale di geofisica e vulcanologia., 2005.

Hall, J.: The 25-m DTM (Digital Terrain Model) of Israel, Isr. J. Earth Sci., 57(3–4), 145–147, doi:10.1560/IJES.57.3-4.145, 2008.

Hall, J. F., Holmes, W. T. and Somers, P.: Northridge earthquake, January 17, 1994, Prelim. Reconnaiss. Rep., 1994.

Hough, S. E. and Avni, R.: The 1170 and 1202 CE Dead Sea Rift earthquakes and long-term magnitude distribution of the Dead Sea Fault Zone, Isr. J. Earth Sci., 58(3), 295–308, doi:10.1560/IJES.58.3-4.295, 2011.

Hough, S. E., Friberg, P. A., Busby, R., Field, E. F., Jacob, K. H. and Borcherdt, R. D.: Sediment-induced amplification and the collapse of the Nimitz Freeway, Nature, 344(6269), 853–855, doi:10.1038/344853a0, 1990.

Joyner, W. B. and Boore, D. M.: Measurement, characterization, and prediction of strong ground motion, 1988.

Kagan, E., Stein, M., Agnon, A. and Neumann, F.: Intrabasin paleoearthquake and quiescence correlation of the late Holocene Dead Sea, J. Geophys. Res. Solid Earth, 116(4), 1–27, doi:10.1029/2010JB007452, 2011.

Miller, R. D., Xia, J., Park, C. B., Survey, K. G., Hunter, J. A. and Harris, J. B.: Comparing Shear-Wave Velocity Profiles Inverted From Multi- Channel Surface Wave With Borehole Measurements, , 18, 181–190, 2002.

Milne, J.: Seismology: London, Kegan Paul, Trench, Truber, 1898.

Moro, G. D.: Surface Wave Analysis for Near Surface Applications., 2015.

Moro, G. D., Pipan, M. and Gabrielli, P.: Rayleigh wave dispersion curve inversion via genetic algorithms and Marginal Posterior Probability Density estimation, , 61, 39–55, doi:10.1016/j.jappgeo.2006.04.002, 2007.

Park, C. B., Miller, R. D. and Xia, J.: Multi-Channel Analysis of Surface Waves (MASW) prepared by., 1997.

Park, C. B., Miller, R. D. and Xia, J.: Imaging dispersion curves of surface waves on multi-channel record, in SEG Technical Program Expanded Abstracts 1998, vol. 17, pp. 1377–1380, Society of Exploration Geophysicists., 1998.

Raphael, K. and Agnon, A.: Earthquakes East and West of the Dead Sea Transform in the Bronze and Iron Ages, 769–798 in Shai et al., 2018.

Ryden, N., Park, C. B., Ulriksen, P. and Miller, R. D.: Multimodal Approach to Seismic Pavement Testing, J. Geotech. Geoenvironmental Eng., 130(6), 636–645, doi:10.1061/(ASCE)1090-0241(2004)130:6(636), 2004.

Shani-Kadmie, S., Tsesarsky, M. and Gvirtzman, Z.: Distributed slip model for forward modeling strong Earthquakes, Bull. Seismol. Soc. Am., 106(1), 93–103, doi:10.1785/0120150102, 2016.

Shapira, A.: Redetermined magnitudes of earthquakes in the Afro-Eurasian Junction, Isr. J. Earth Sci, 28, 107–109, 1979.

Shapira, A., Avni, R. and Amos, N.: A new estimate for the epicenter of the Jericho earthquake of 11 July 1927, Isr. J. Earth-Sciences, 42(2), 93–96, 1993.

Singh, S. K., Lermo, J., Dominguez, T., Ordaz, M., Espinosa, J. M., Mena, E. and Quaas, R.: The Mexico earthquake of September 19, 1985-A study of amplification of seismic waves in the valley of Mexico with respect to a hill zone site, Earthq. spectra, 4(4), 653–673, 1988.

The Standards Institution of Israel: Design provisions for earthquake resistance of structures - SI 413, , (5), 2013.

Willis, B.: Earthquakes in the Holy Land, Bull. Seismol. Soc. Am., 18(2), 73–103, 1928.

Xia, J., Miller, R. D. and Park, C. B.: Estimation of near-surface shear-wave velocity by inversion of Rayleigh waves, Geophysics, 64(3), 691–700, doi:10.1190/1.1444578, 1999.

Zaslavsky, Y.: Questioning the applicability of soil amplification factors as defined by NEHRP (USA) in the Israel building standards, Nat. Sci., 04(28), 631–639, doi:10.4236/ns.2012.428083, 2012.

Zohar, M. and Marco, S.: Re-estimating the epicenter of the 1927 Jericho earthquake using spatial distribution of intensity data, J. Appl. Geophys., 82, 19–29, doi:10.1016/j.jappgeo.2012.03.004, 2012.

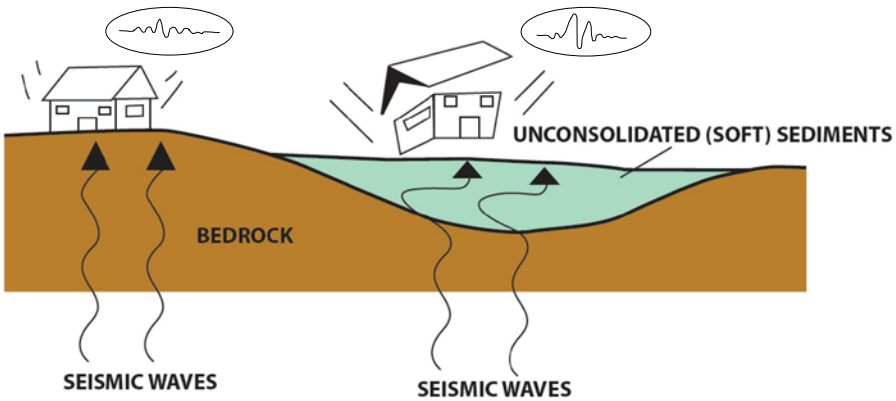

Figure 1: Schematic view of site amplification. Seismogram at the surface shows amplification in comparison to the seismogram located over the bedrock (modified after Ciaccio and Cultrera, 2014).

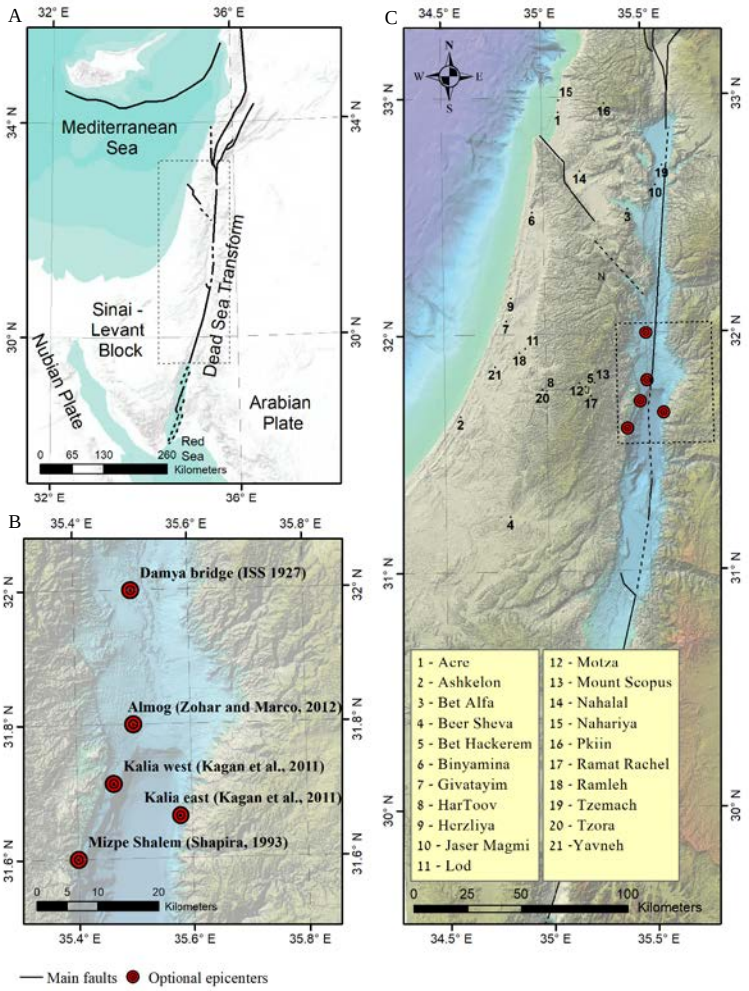

Figure 2: Research area: A) Middle East area with the main tectonic elements. B) Proposed epicenters for the 1927 earthquake event with all sites that were investigated placed over a 25m DTM image (Hall, 1996). C) Detailed location of the proposed epicenters. Also shown are sites mentioned in the text: Jerusalem (J) and Nablus (N).

5

Figure 3: Wreckage of the Winter Palace Hotel, Jericho, after the 1927 earthquake. American Colony (Jerusalem). Photo Dept., photographer.

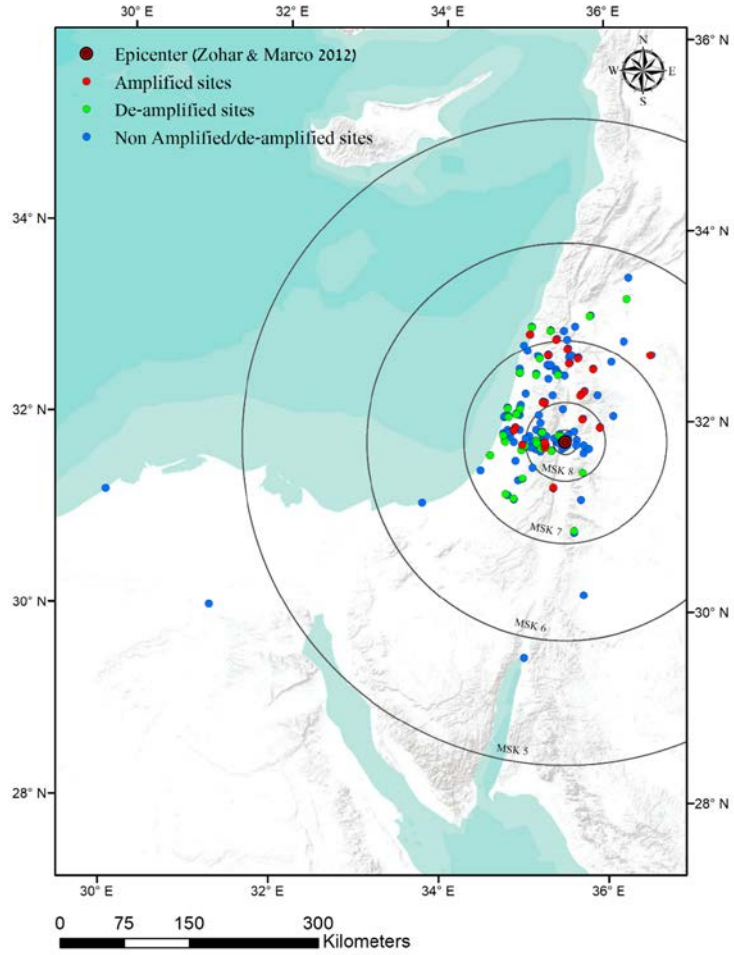

Figure 4: Isoseismal map. The epicentral locations in red and black circles. Red and green dots are suspect amplified or de-amplified sites (respectively). Blue dots are sites which have MSK values expected from the attenuation equation (with 60% prediction boundary).

5

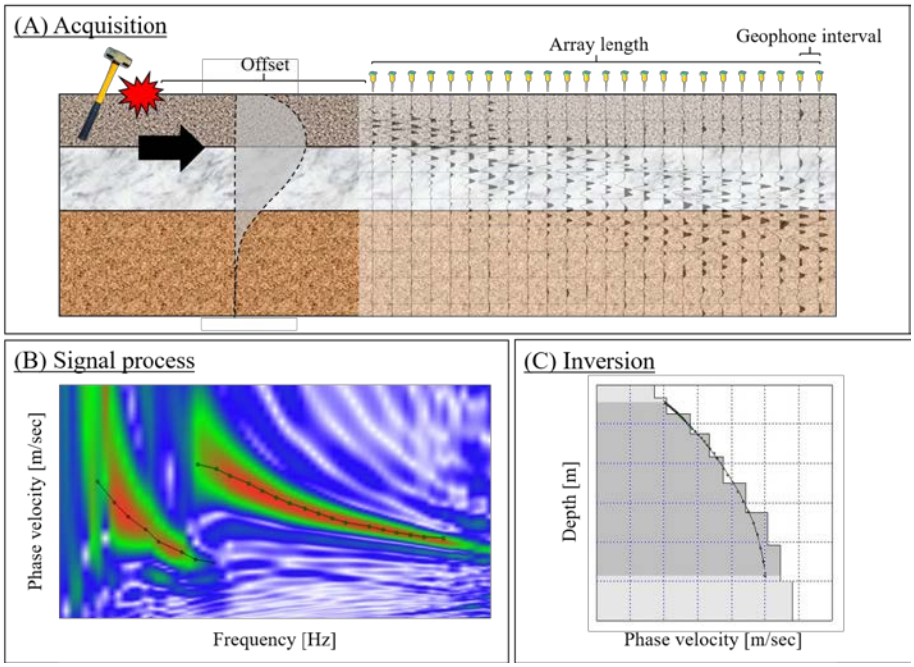

Figure 5: Multichannel Analysis of Surface Waves (MASW) technique: A. Acquisition – Using a sledgehammer as an artificial source and a linear array of geophones that receives all wavelets. B. Signal process – A fundamental mode and first higher mode over the dispersion image. C. Inversion – Final V_s profile which best fits the dispersion curve.

5

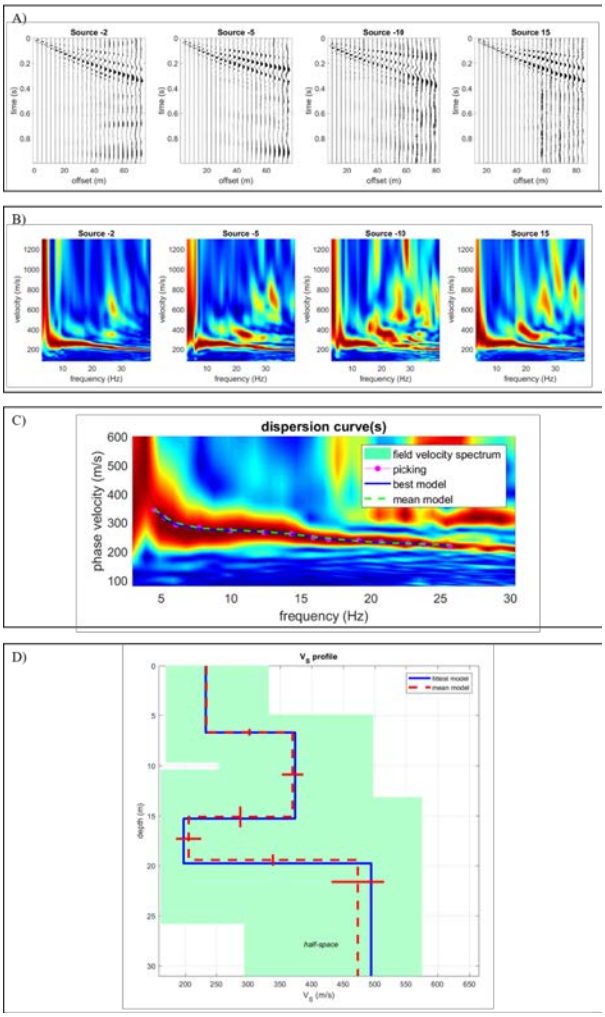

Figure 6: Data processing (example from Binyamina): A – Raw data of four different offsets. B – The four relative dispersion images calculated from the raw data. C – Best dispersion Image (offset 15): pink dots are the analyst's dispersion curve picking. The blue line and yellow dashed line are respectively the best and the mean curves from the final model,. D – Shear-wave velocity model (Blue profile for the best one and red dashed line is the mean profile from 100 lower RMS.

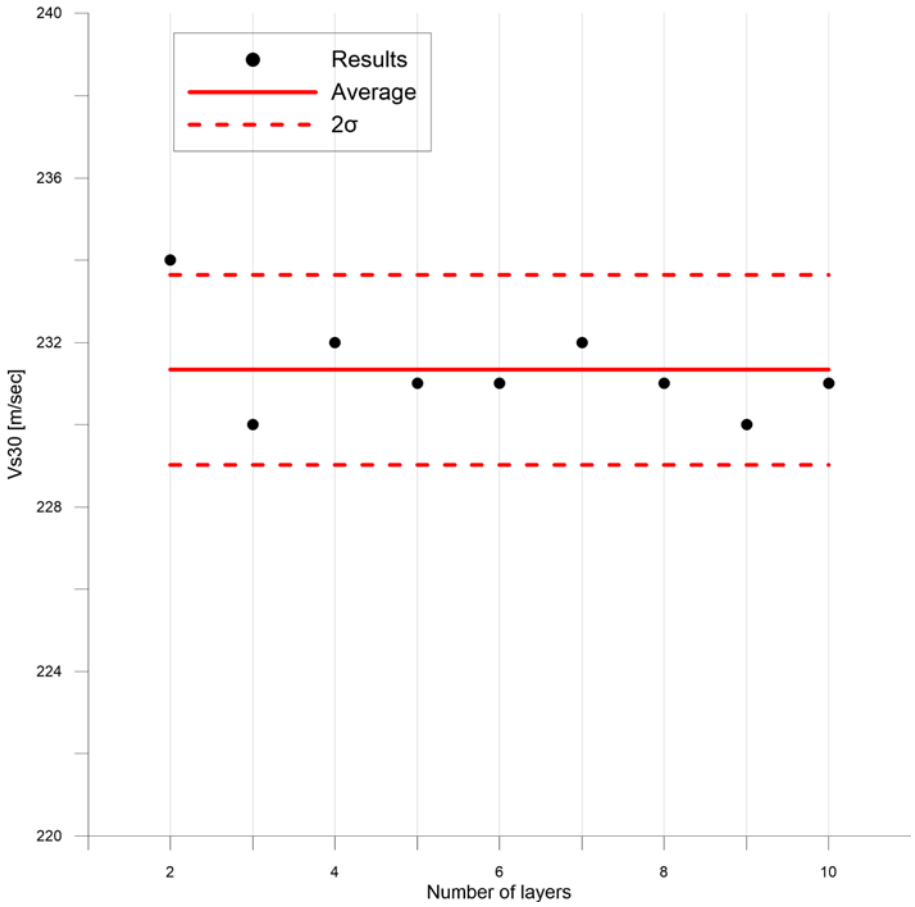

Figure 7: Vs_{30} as a function of a number of layers (example from Beit Alfa).

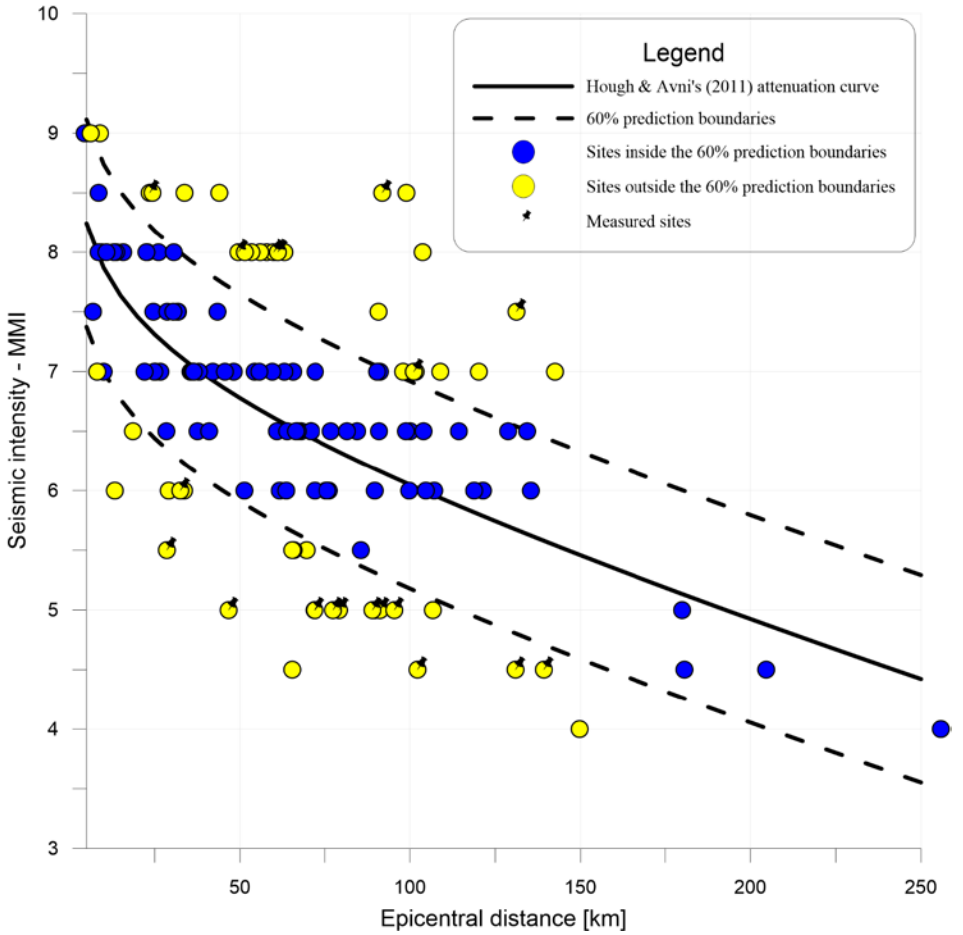

Figure 8: Avni's seismic intensity (MMI) estimates of all the 133 sites. Distance is corrected according to the Zohar & Marco epicenter. Yellow dots are suspected amplified or de-amplified sites. Sites with pins are sites where we measured the *Vs* profile. Blue dots are sites which have MSK values expected from the attenuation equation (within the 60% prediction boundary).

5

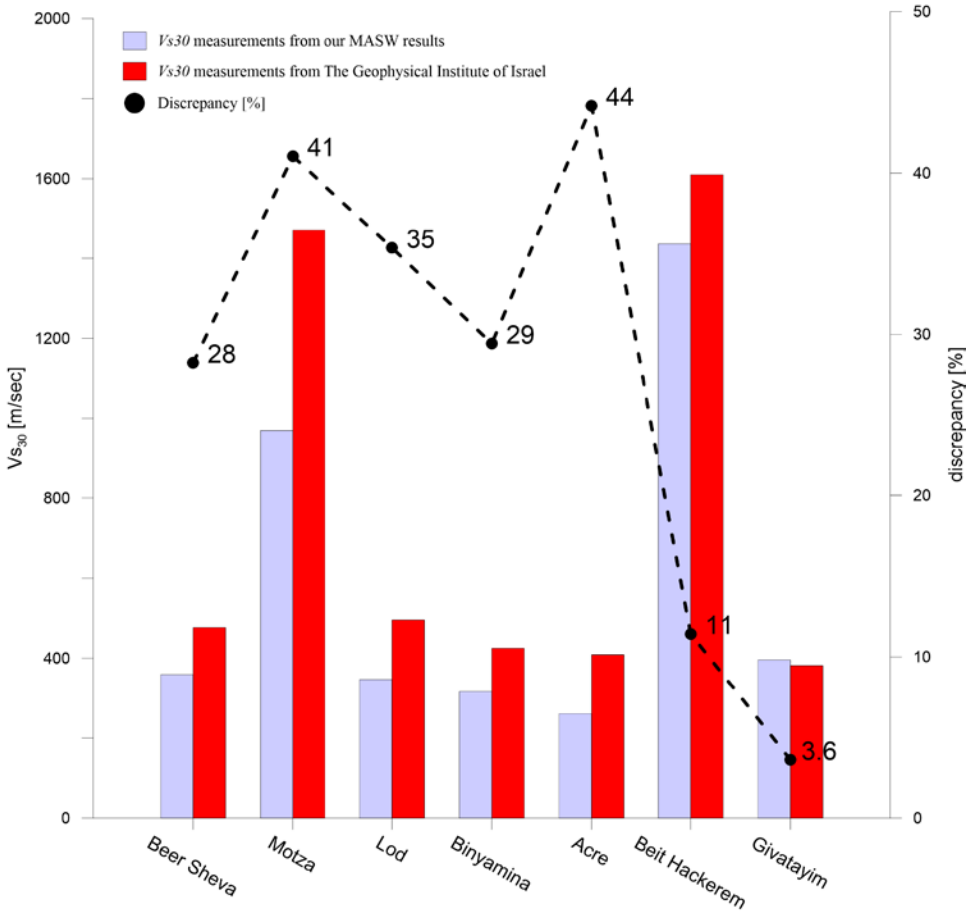

Figure 9: Comparison between our Vs_{30} results (light blue) and those calculated from GII's report (red) (Aksinenko and Hofstetter, 2012).

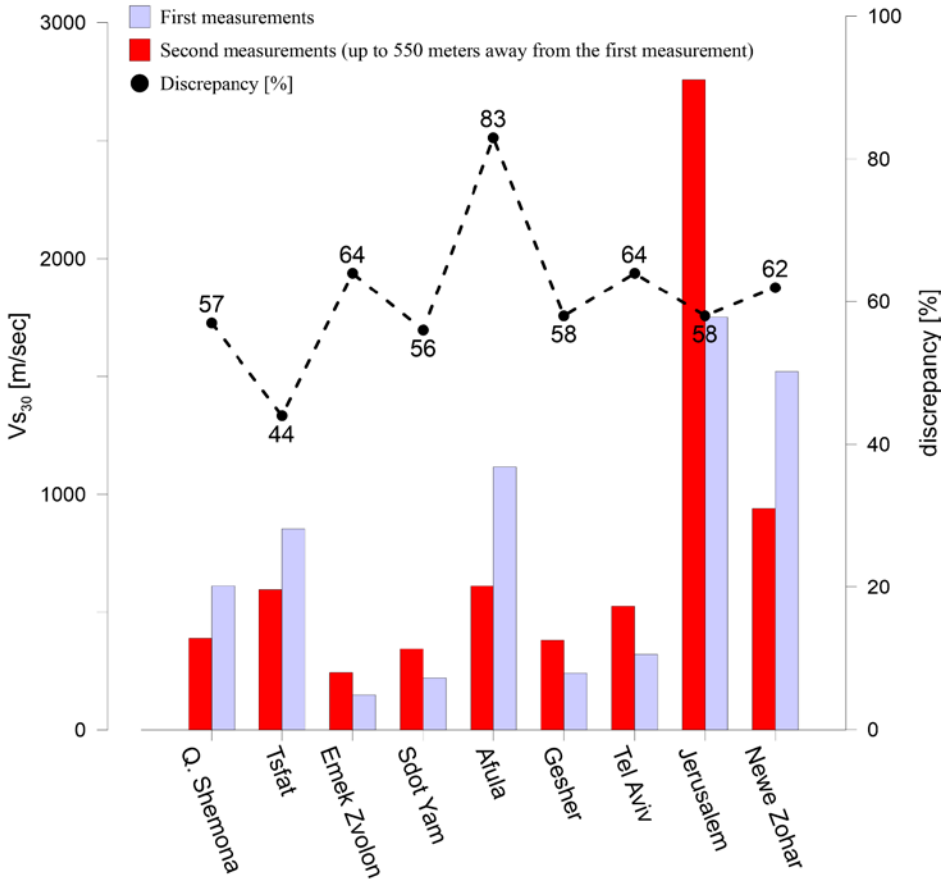

Figure 10: Comparison between GII's closest measurements (up to 550 meters).

Formatted: Normal

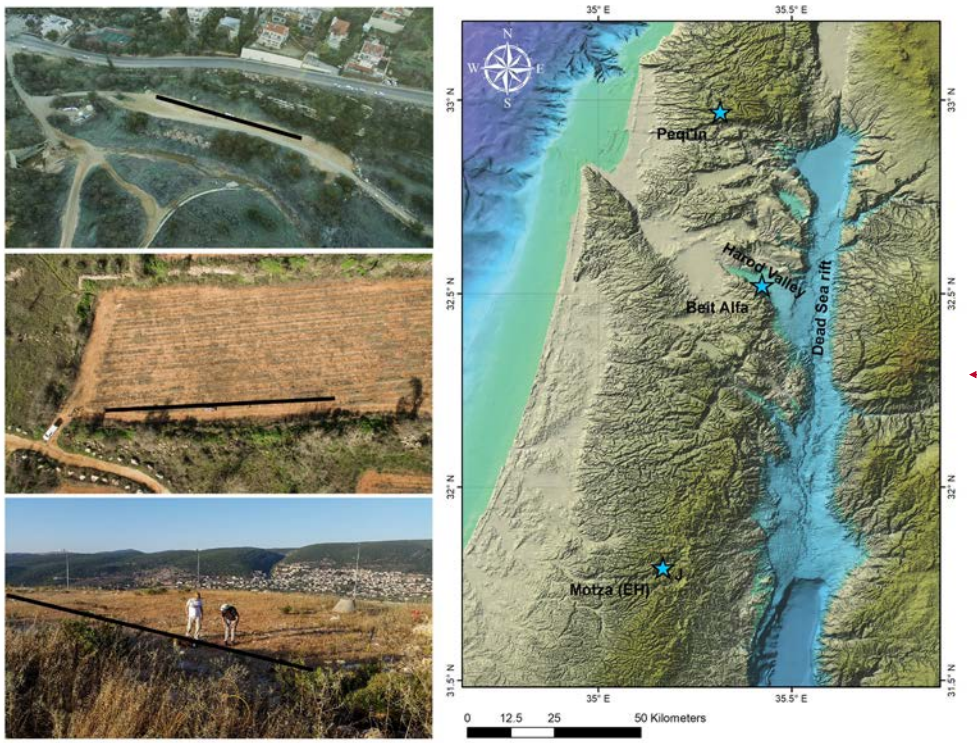

Figure 11: Three of the sites investigated: A) Motza 1, B) Motza 2, and C) Peqi'in. Black lines represent the seismic line location. D) The locations of the sites over a 25m DTM image (Hall, 1996). Also shown are sites mentioned in the text: Jerusalem

Formatted: Keep with next

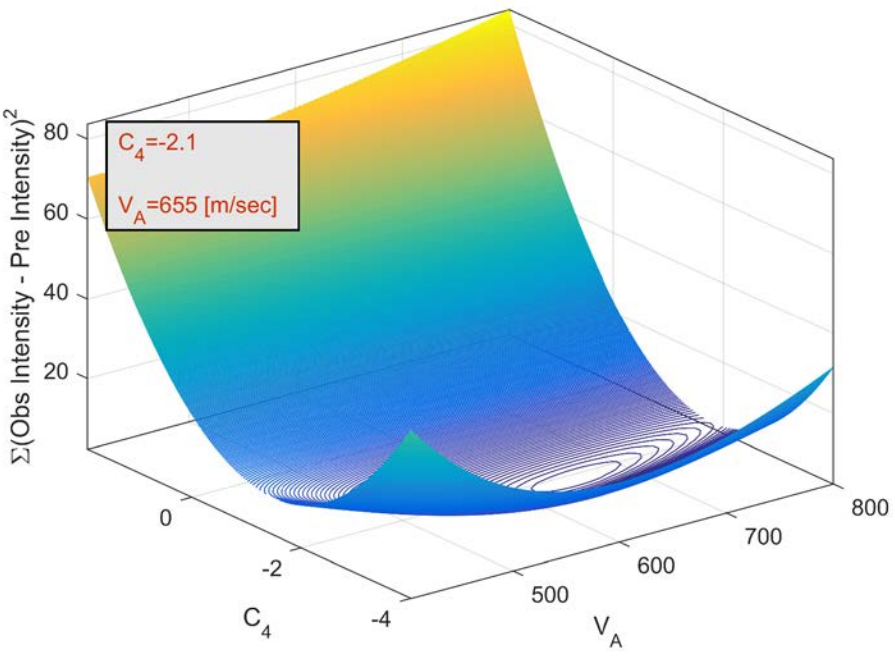

Figure 12: A Sensitivity analysis for calibration of the new equation.

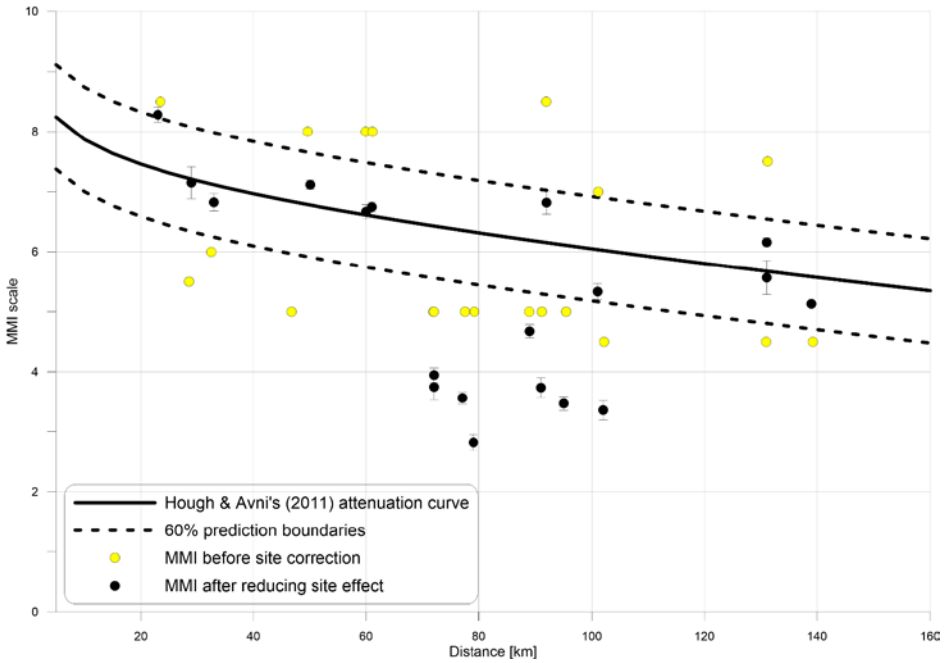

Figure 13: Site response corrections: Yellow dots are MMI before site correction and black dots with error bars due to *Vs* uncertainty, represent the MMI after reducing site effects.

Acquisition parameters

Number of geophones	24
Geophone spacing	2-3 meters
Array length	46-69 meters
Sampling rate	8 kHz
Record length	0.5-2 second
Receivers	4.5 Hz vertical
Source	5 kg hammer

Table 1: Acquisition parameters.

ID	Site	Vs_{30} [m/sec]	Error [%]	Epicentral distance
1	Acre	261	13	131
2	Ashkelon	561	5	89
3	Be'er Sheva	359	8	91
4	Beit Hakerem	1436	12	29
5	Beit Alfa	232	5	79
6	Binyamina	316	5	95
7	Givatayim	396	6	72
8	Herzliya	330	5	77
9	Jasar-Majami	294	9	92
10	Lod 1	320	4	60
11	Lod 2	374	6	
12	Motza 1	1065	8	33
13	Motza 2	874	8	
14	Mt. Scopus 1	600	6	23
15	Mt. Scopus 2	582	5	
16	Nahalal	380	7	102
17	Nahariya	883	1	139
18	Peqi'in	1444	3	131
19	Ramleh	360	4	61
20	Tzemach 1	281	5	101
21	Tzemach 2	273	4	
22	Tzora	430	3	50
24	Yavneh	361	10	72

Table 2: MASW results.